

Experimental and modelling study of pulsed optically stimulated luminescence in quartz, marble and beta irradiated salt

V Pagonis^{1,4}, S M Mian¹, M L Chithambo², E Christensen³ and C Barnold¹

¹ Physics Department, McDaniel College, Westminster, MD 21158, USA

² Department of Physics, Rhodes University, PO Box 94, Grahamstown 6140, South Africa

³ Physics Department, Virginia Tech, VA 24061, USA

E-mail: vpagonis@mcdaniel.edu

Received 10 October 2008, in final form 19 December 2008

Published 19 February 2009

Online at stacks.iop.org/JPhysD/42/055407

Abstract

Optical stimulation luminescence (OSL) signals can be obtained using continuous-wave optical stimulation (CW-OSL), the linear modulation optical stimulation method (LM-OSL) and the time-resolved optical stimulation (TR-OSL) method. During TR-OSL measurements, the stimulation and emission of luminescence are experimentally separated in time by using short light pulses. This paper presents new TR-OSL data for annealed high purity synthetic quartz, for marble and for commercially available iodized salt. A new type of behaviour for TR-OSL signals for quartz and iodized salt is presented, in which the OSL signal exhibits a nonmonotonic behaviour during optical stimulation; this type of behaviour has not been reported previously in the literature for quartz. Furthermore, a luminescence component with very long luminescence lifetime is reported for some quartz aliquots, which may be due to the presence of a delayed-OSL (DOSL) mechanism in quartz. A new kinetic model for TR-OSL in quartz is presented, which is based on a main electron trap and on several luminescence centres. The model is used to quantitatively fit several sets of experimental data of pulsed optically stimulated luminescence from quartz.

1. Introduction

The technique of optical stimulation of luminescence (OSL) is a well-established and commonly used method for dating and dosimetry applications [1]. There are three common procedures for measuring OSL signals, namely, the continuous-wave optical stimulation (CW-OSL), the linear modulation optical stimulation method (LM-OSL) developed by Bulur *et al* [2] and the time-resolved optical stimulation (TR-OSL), sometimes also referred to as pulsed optical stimulation (see, e.g. Bøtter-Jensen *et al* [3] and references therein). During TR-OSL measurements, the stimulation and emission of luminescence are experimentally separated in time by using a short light pulse. The main advantage of TR-OSL measurements over CW-OSL measurements is that only a negligible proportion of the optically active charge is sampled

during a TR-OSL measurement, so that luminescence can be measured several times without significantly depleting the traps. This technique allows measurements of luminescence lifetimes and thus a means to estimate the delay between stimulation and emission of luminescence.

Time-resolved optically stimulated luminescence spectra presented in this paper should not be mistaken for decay curves produced in CW-OSL. A CW-OSL decay curve displays the change in luminescence intensity with the duration of stimulation, whereas TR-OSL data display the delay between stimulation and luminescence emission [3, 11]. The TR-OSL spectra should also not be confused with time-resolved luminescence spectra found in optical absorption studies or photoluminescence spectrometry where the luminescence intensity is plotted as a function of the emission wavelength or the photon energy.

TR-OSL measurements have been carried out rather extensively in quartz and feldspar samples, due to the

⁴ Author to whom any correspondence should be addressed.

importance of these materials in dating and retrospective dosimetry. Additionally, this technique has been applied in the study of feldspars, as a dosimetry tool for $\text{Al}_2\text{O}_3:\text{C}$, and in studies of limestone (see, e.g., Chithambo [4, 5] and references therein). Chithambo [6] studied the temperature related changes in luminescence lifetimes and luminescence intensity in the 'fast', 'medium' and 'slow' component regions of OSL signals from quartz. The luminescence signal was found to increase for temperatures between 20 and 100 °C, with a subsequent decrease up to 200 °C. The corresponding luminescence lifetimes remained constant up to 100 °C and then decreased up to 200 °C. These results allowed estimations of the activation energies for thermal quenching and for thermal assistance effects in quartz, for the 'fast', 'medium' and 'slow' OSL components in quartz. Chithambo [7] examined the properties of luminescence lifetimes in quartz for annealing temperatures between 500 and 900 °C, and for varying annealing times. The lifetimes decreased with annealing temperature from 500 to 900 °C, but in the interval 800–900 °C lifetimes remained essentially constant. These results were discussed within the framework of the luminescence emission process involving at least two luminescence centres.

Time-resolved infrared OSL signals have also been studied consistently in feldspars since the first such investigations on alkali feldspars by Sanderson and Clark [8] who used a 10 ns pulse from a laser set at 470 nm. This was followed by exploratory measurements of lifetimes from both alkali and plagioclase feldspars by Clark and Bailiff [9] and a substantive study on lifetimes and emission spectra of the same materials by Clark *et al* [10] using, in both cases, a 5 ns pulse and laser stimulation at 850 nm. In the latter, Clark *et al* [10] considered the role of impurities and electron–hole recombination at lattice defects and suggested the latter as the more likely to explain the luminescence emission from feldspar. The possibility of measuring pulsed luminescence from feldspar using longer pulsed widths was demonstrated by Chithambo and Galloway [11] who used both 50 and 4.4 ns from pulsed 525 nm green LEDs on alkali feldspars. Recently, Tsukamoto *et al* [12] studied the time-resolved infrared OSL signals from K- and Na-feldspar samples extracted from sediments using pulsed IR stimulation. These authors found that the relative contribution of long lifetime components in K-feldspars is greater than that in Na-feldspars, consistent with the results of Clark *et al* [10], and compared the pulsed and continuous-wave equivalent doses obtained from four feldspar samples. Denby *et al* [13] suggested using the differences in the pulsed-OSL signals from quartz and feldspars when dealing with either mixed quartz/feldspar mineral samples or in the case of quartz contaminated with feldspars. These authors suggested a technique of gating the counting period, to significantly reduce the feldspar signal relative to the signal from quartz.

Chithambo [4, 5], in a pair of recent papers, presented a theoretical framework for analysing and interpreting time-resolved luminescence data, and developed equations for optimizing the performance of a TR-OSL system. In the second paper Chithambo [5] compared experimental results and computer simulations with the conceptual models

discussed in the first paper, and demonstrated the calculation of luminescence lifetimes by using exponential functions, while the use of stretched-exponential functions was also considered. The effect of thermal quenching on the luminescence lifetimes was discussed at length, and various methods for calculating the activation parameters were described. Chithambo *et al* [14] studied TR-OSL of low sensitivity natural quartz from crystalline rock. These authors found evidence of a weak short lifetime component in several samples. They also found considerable variation in the values of the principal luminescence lifetimes for various types of quartz and attributed these large variations to different thermal histories of the samples. The results were explained in terms of a model consisting of three luminescence centres, with the thermal history of the sample possibly linked to the hole concentration of the centres. Ogundare and Chithambo [15] studied the luminescence lifetimes and luminescence intensity from TR-OSL data from annealed and unannealed quartz samples from Nigeria. The measurements were carried out for various annealing temperatures, irradiation doses and measurement temperatures. The activation energies for thermal quenching and thermal assistance were evaluated and the experimental results were interpreted using a model consisting of three luminescence centres.

There have also been some recent studies of a variety of signals from common iodized salt. Murthy *et al* [16] studied the thermoluminescence (TL) characteristics of common iodized salt and suggested that it can be used as an 'accidental dosimeter' in the case of a nuclear accident. These authors observed three well-resolved TL peaks at 133, 205 and 238 °C. Ankjærgaard *et al* [17] studied electron emission during thermal stimulation using a Geiger–Müller electron detector. They measured simultaneously optically stimulated electrons (OSEs), thermally stimulated electrons (TSEs), optically stimulated luminescence (OSL) and TL from natural minerals including common salt. Bulur *et al* [2] studied OSL signals from various insulators including quartz and NaCl using the LM-OSL technique. They studied the initial decay rate of the blue 470 nm stimulating light and tested the relation between the detrapping rates and the stimulation light intensity. Their results showed that the detrapping rate of the OSL signal from NaCl varied non-linearly with the stimulation intensity. Bailey *et al* [18] performed a detailed study of the luminescence properties of NaCl, based on the OSL signal in the UV region, when the samples were stimulated using light at 420–560 nm. These authors presented experimental results for signal resetting, dose response and thermal stability. Optical exposure resulted in fast signal resetting, and they found no TL or OSL signals present after re-crystallization. They suggested the possibility of using these OSL signals for dating natural salt deposits. Thomsen *et al* [19] presented LM-OSL data from a variety of household and workplace chemicals including common salt, and investigated the possibility of using them as retrospective luminescence dosimeters.

To the best of our knowledge, there have been no published reports of TR-OSL data for common salt.

The purpose of this paper is to present TR-OSL data for a variety of materials obtained using a TR-OSL system

constructed using relatively inexpensive and commercially available components. Results are presented for high purity synthetic quartz, for annealed marble, for beta irradiated iodized salt and for the important dosimetric material $\text{Al}_2\text{O}_3 : \text{C}$. A new type of nonmonotonic behaviour is presented for quartz and iodized salt samples, not previously reported in the literature. A new type of kinetic model is presented which is used to quantitatively fit several sets of experimental data, demonstrating different TR-OSL behaviours for quartz samples under different experimental conditions.

2. Experimental

Measurements of time-resolved luminescence intensities were made with a pulsed-OSL system constructed using commercially available components. The LED pulsing system consists of a T-Cube LED Driver (Model LEDD1 manufactured by THORLABS Inc.), which has a maximum flash frequency of 10 kHz, minimum strobe pulse width of $50 \mu\text{s}$ and a strobe turn-on/turn-off time shorter than $25 \mu\text{s}$. A system of 16 blue LEDs ($\sim 470 \text{ nm}$) delivers a nominal power of $\sim 16 \text{ mW cm}^{-2}$, according to the data provided by the manufacturer. The system also contains a frequency generator, a photomultiplier tube (EMI type 9635QA), associated electronics for pulse processing and a multichannel scaler for data collection and analysis. A multichannel scaler (ORTEC MCS-plus) is used for data collection, with a minimum dwell time of $2 \mu\text{s}$. The trigger signal for data acquisition is provided by a frequency generator, which also provides the square wave frequency necessary for pulsing the LED system. Data collection is synchronized to the start of a sweep from the MCS, with the MCS automatically advancing to the next channel at the end of the dwell time. The final time-resolved luminescence intensity consists of a plot of cumulative photon counts against time. There is negligible deadtime between channels and each run consists of 100 000 sweeps.

Luminescence was stimulated at a pulse width of 100 or $200 \mu\text{s}$ per sweep and time-resolved luminescence data were recorded over a dynamic range of 600 or $1200 \mu\text{s}$.

Time-resolved curves are constructed experimentally by adding many simple curves of identical shape. Each sweep is over the full dynamic range (600 or $1200 \mu\text{s}$ in our experiments), and the data from thousands of such sweeps are added together to form the curves shown in figures 2–4. A pulse width of $100 \mu\text{s}$ and a dynamic range of $600 \mu\text{s}$ mean that the light stimulation will be on for $100 \mu\text{s}$ and off for $500 \mu\text{s}$. This is necessary because the signal from individual curves is too weak to be measured, and summation of many weak signals produces a measurable strong TR-OSL signal.

It is noted that the experimental procedure described here is different from the one used, for example, in some commercial TL/OSL readers, in which the on-time data are gated off and only the off-time data are collected in a single sweep. This gating of the on signal is necessary because the high intensity light during this period will result in damage to the photomultiplier tube. Detailed features of instrumentation

for measurement of time-resolved luminescence from quartz have been presented, e.g. in [21–23]. The features of pulsing systems and measurement procedures have also been discussed by many authors, e.g. [3, 10, 11, 21].

Luminescence was detected in the spectral region 340–380 nm (FWHM) by a photomultiplier tube (EMI type 9635QA) using a standard combination of optical filters used for OSL systems, namely, a Schott BG39 filter with a transmission band 340–620 nm and a UG11 filter with a transmission band in the region 270–380 nm. Time-resolved luminescence data were recorded at room temperature, with no chemical treatment of the quartz and common salt samples. Some of the quartz and marble samples were annealed for various annealing times at temperatures in the region 800–900 °C, as discussed in the relevant sections. The powder samples used for TR-OSL measurements were deposited on aluminium discs of 1.5 cm diameter. The background signal was measured before each measurement and was digitally subtracted from the data. The samples of high purity synthetic quartz of the premium Q-type (Sawyer Research Products), were crushed, ground and sieved and the 60–90 μm grain size was selected.

The reported TL glow curves for common salt were measured using conventional Daybreak TL equipment, with a HA-3 infrared-rejecting filter to reduce thermal noise and a 9635QA photomultiplier tube for photon counting. All TL glow curves were recorded with a linear heating rate of 2°C s^{-1} under constant nitrogen flow. The powder samples were irradiated on-plate using a 100 mCi Sr-90 source with a nominal dose rate of 2 Gy min^{-1} . Black body radiation was digitally subtracted from the TL glow curves. The TL glow curves were recorded using narrow band interference filters (from Oriel Corporation), with peak transmissions located at intervals of 20 nm in the 400–600 nm region. The transmission coefficients of the filters are typically between 20% and 50%, with a very narrow transmission band with a FWHM of $\pm 5 \text{ nm}$.

3. Experimental results

3.1. TR-OSL data for $\text{Al}_2\text{O}_3 : \text{C}$

Figure 1(a) shows TR-OSL data for the well-known dosimetric material $\text{Al}_2\text{O}_3 : \text{C}$, demonstrating the accuracy and performance of the experimental setup. The powder sample was irradiated for 1 min with a nominal beta dose of 2 Gy, and the time-resolved OSL intensity was measured for seven consecutive cycles consisting of 100 000 scans each, followed by a 15 s interval between each cycle. During the 15 s interval between cycles, the sample continued to be exposed to the TR-OSL signal from the LEDs, causing further depletion of the charge concentrations in the traps and in the recombination centres. The overall signal in figure 1(a) decreases for each of the seven cycles, due to this partial depletion of the traps and/or recombination centres available in the material. The bottom graph in figure 1(a) indicates the level of the background during these measurements and is seen to be very small compared with the TR-OSL signal. The background signal during the light pulse consists of photomultiplier noise and scattered

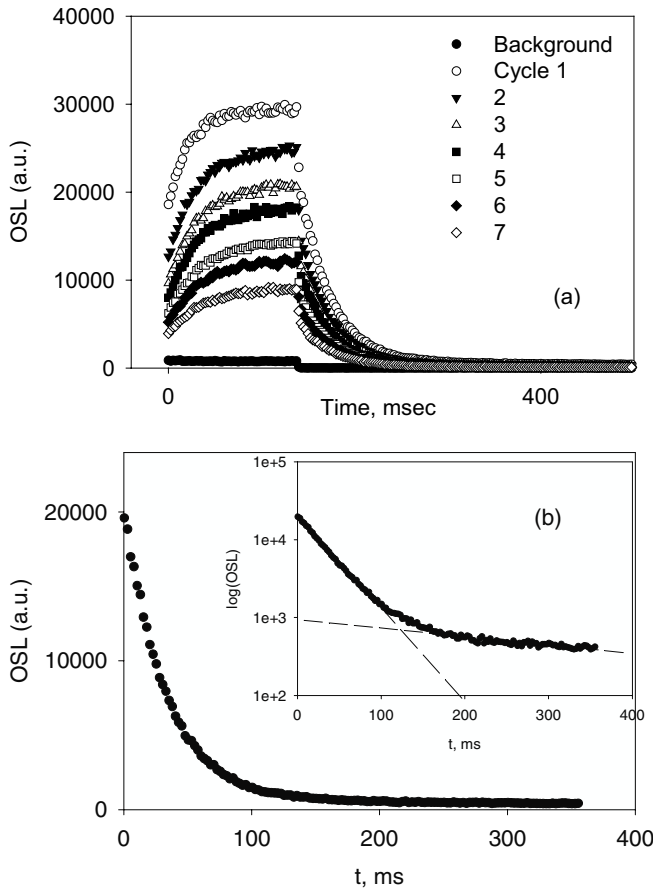


Figure 1. (a) Time-resolved data for a sample of $\text{Al}_2\text{O}_3:\text{C}$. (b) One of the graphs in (a) is fitted to two decaying exponential corresponding to the ‘fast’ and ‘slow’ components.

stimulating light, but only consists of photomultiplier noise after the light pulse.

Figure 1(b) shows the portion obtained while the LEDs were off for one of the time-resolved data of figure 1(a), fitted with two decaying exponential functions. The inset shows the same data on a logarithmic scale, demonstrating the two exponential decay components. The time constant for the first ‘fast’ component in the signal was found to be constant for all seven cycles in figure 2(a), with an average lifetime of $\tau = (33.0 \pm 0.2)$ ms. The time constant for the second ‘slow’ component in the signal was found to gradually decrease from a value of 928 ms for cycle 1 to a value of 320 ms for cycle 7. These values compare well with the results obtained by Markey *et al* [20] and Akselrod and McKeever [21], who reported a value of ~ 35 ms for the fast component and a value of ~ 545 ms for the slower component at room temperature. These authors also reported that the lifetime of the faster component corresponds to the F-centre lifetime, while the lifetime of the slower component is a function of the temperature. This second slower component is assumed to be due to trapping of charges in two shallow traps (STs) during optical stimulation (see, e.g. Bøtter-Jensen *et al* [3, p 59] and references therein). This luminescence component is also termed a delayed-OSL (DOSL) emission, and is presumably caused by the charge leaking slowly out of the STs, and recombining at the luminescence centre.

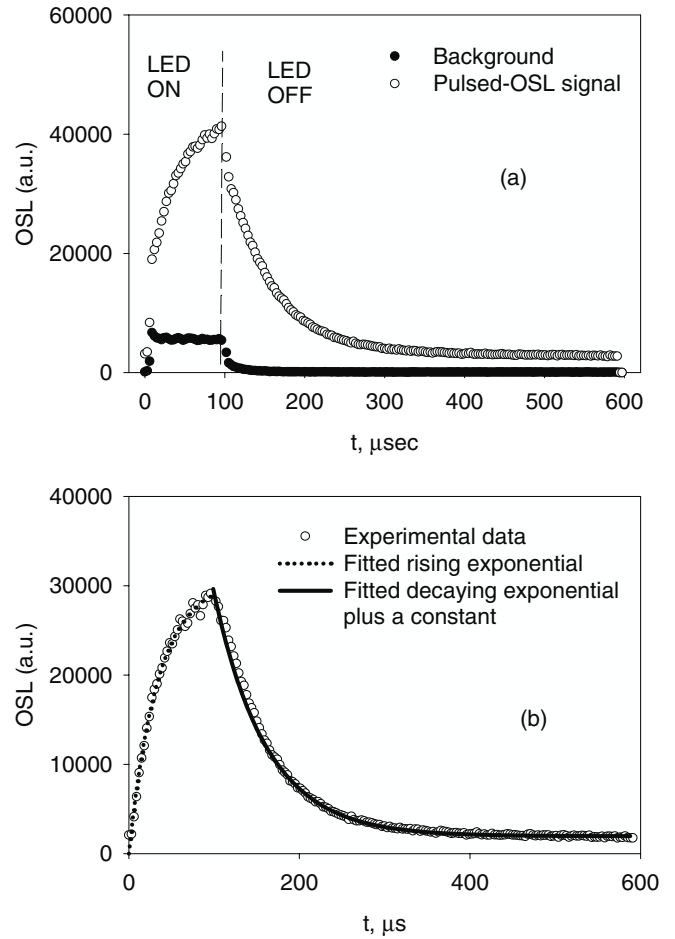


Figure 2. (a) Time-resolved OSL intensity for high purity synthetic quartz. The sample was annealed at 900°C for 1 h. (b) The rising and decaying parts of the signal shown in (a) are fitted with a rising exponential and a decaying exponential plus a constant correspondingly, yielding a lifetime $\tau_R = (34.0 \pm 0.1)$ μs for the rising part, and a luminescence lifetime of $\tau_d = (61.1 \pm 0.6)$ μs for the decaying part of the signal.

3.2. TR-OSL data for synthetic Q-quartz

Figure 2(a) shows an example of a time-resolved measurement for a sample of high purity synthetic quartz. The TL properties of this material were studied previously in detail (Charitides *et al* [22], Kitis *et al* [23], Polymeris *et al* [24]). The sample was annealed for 1 h at 900°C and subsequently irradiated for 5 min with a beta source, for a nominal dose of 10 Gy. The time-resolved data were measured immediately after the end of the irradiation. The rather high background signal in this example consists of scattered luminescence-excitation light and is subtracted digitally from the signal. By following the analysis suggested by Chithambo [4, 5], the data up to 100 μs were fitted with a single rising exponential curve (while the LED is on), and with a decaying exponential plus a constant while the LED is off. The latter constant is added to account for the background. The resulting fits are shown in figure 2(b) and the time constants obtained from the fitting procedure were $\tau_R = (34.0 \pm 0.1)$ μs for the rising part and $\tau_d = (61.1 \pm 0.6)$ μs for the decaying part of the signal. The method of fitting suggested by Chithambo [4] should produce the same

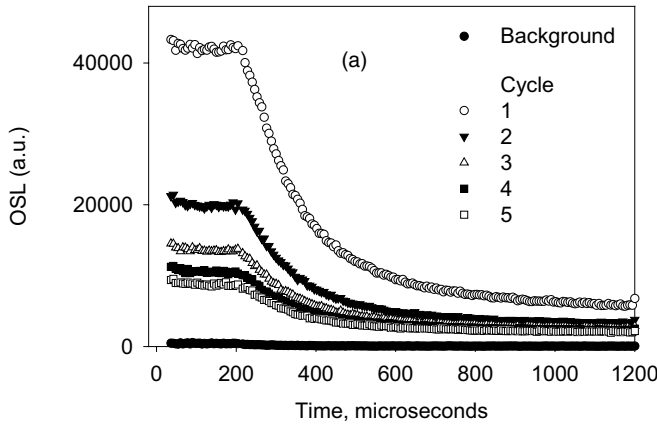


Figure 3. (a) A set of TR-OSL data for annealed synthetic quartz, recorded at a much higher light stimulation intensity than in figure 2. The background signal is seen to be negligible compared with the luminescence signal. This TR-OSL intensity consists of five consecutive cycles consisting of 100 000 scans each, with a 15 s stimulation interval between each cycle. All the graphs can be fitted with a decaying exponential plus a constant. The resulting average time constant τ_f is $\tau_f = (132 \pm 4) \mu\text{s}$.

time constant from either portion of the time-resolved OSL intensity if only one such lifetime is dominant. That the values differ in our data suggests that the synthetic quartz sample has multiple lifetime components with one probably much longer than the pulse width. It is noted that several values of τ_d in the range 30–100 μs have been reported for a variety of quartz samples (Chithambo [6], Ogundare and Chithambo [15]). This wide variation in luminescence lifetimes is usually attributed to the different thermal and irradiation histories, as well as the varying provenance of quartz samples. In a subsequent section of this paper it will be shown that the experimental data in figure 2 can also be fitted using a kinetic model involving one electron trap and several luminescence centres in quartz.

Figure 3 shows a different example of a time-resolved measurement for another aliquot of high purity synthetic quartz. This measurement was recorded at a much higher light intensity than the data of figures 1 and 2, by exposing the sample to the full power of the LED system. The sample was annealed for 1 h at 900 °C and subsequently irradiated for 10 min for a nominal dose of 20 Gy. The bottom graph in figure 3(a) represents the background signal, which is seen to be negligible compared with the luminescence signal both during and after the optical stimulation pulse. This time-resolved OSL intensity was measured for five consecutive cycles consisting of 100 000 scans each, followed by a 15 s interval between each cycle while the LED was continuously stimulating the sample. As in figure 1, the overall signal in figure 3 decreases for each successive cycle, due to partial depletion of the traps and/or recombination centres available in the quartz sample. The data in figure 3(a) up to 200 μs is almost constant for all five cycles. The data while the LED is off were fitted with a decaying exponential curve plus a constant. The resulting time constant τ_f describing the data in figure 3 is found to be constant for all cycles within experimental accuracy, with an average value of $\tau_f = (132 \pm 4) \mu\text{s}$. It is noted that this value of the time constant is more than

twice as large as the value of $\tau_d = (61.1 \pm 0.6) \mu\text{s}$ obtained from the data of figure 2, even though the two measurements were carried out using different aliquots of the same synthetic quartz sample. The presence of these two different lifetimes is a strong indicator that several recombination centres may be present in this material, in agreement with the results of several previous studies of quartz which were mentioned in the introduction section. In the next section the experimental data in figure 3 will also be fitted quantitatively using the proposed kinetic model for quartz.

Figure 4 shows yet a different type of result for another aliquot of high purity synthetic quartz, annealed for 1 h at 900 °C and irradiated with a nominal dose of 20 Gy. The background signal in this example is again negligible compared with the luminescence signal, and the OSL intensity was measured for four consecutive cycles consisting of 100 000 scans each, with a 15 s interval of stimulation between cycles. In this example the overall signal in each cycle increases initially and then decreases, while the LED stimulation is still on. This type of non-monotonic behaviour of the TR-OSL signal from quartz is a new experimental result, not reported previously in the TR-OSL literature for quartz. Furthermore, figure 4 shows that not only does the overall signal decrease for each successive cycle but also the time t_{max} corresponding to the maximum of the luminescence signal shifts systematically from $\sim 50 \mu\text{s}$ for cycle 1 to $\sim 190 \mu\text{s}$ for cycle 4. A possible explanation for this systematic shift of the t_{max} is provided in the modelling section.

The data in figure 4 for the time interval when the LED is off, can be fitted with a double exponential curve to yield two different lifetimes, which will be referred to as fast and slow lifetimes. The resulting time constant τ_1 of the first fast component is constant for all cycles within the accuracy of the experimental data, with an average value of $\tau_1 = (180 \pm 50) \mu\text{s}$. The large statistical spread of this value indicates that this component is most likely identical to the fast component found in figure 3, which has a lifetime of $\tau_f = (132 \pm 4) \mu\text{s}$. The lifetime for the second slow component present in the data of figure 4 is very long, with an average value of $\tau_2 = (14 \pm 8) \text{ms}$. This long lifetime indicates that this component must be of a different nature, and that most probably a different mechanism must be involved in producing this luminescence component. One possible explanation for this very high value of the lifetime is that this slow luminescence component may be due to the phenomenon of delayed-OSL signals, which have been reported in several dosimetric materials, including quartz (Bøtter-Jensen *et al* [3, p 59]). This high value of the lifetime has been interpreted as a delayed-OSL effect due to the slow release of charge from STs, followed by recombination at the luminescence centres.

In summary, the experimental data in figures 2–4 are consistent with the presence of at least two components in the TR-OSL data of synthetic quartz, with average lifetimes of $\tau_d = (61.1 \pm 0.6) \mu\text{s}$ and $\tau_f = (132 \pm 4) \mu\text{s}$. The presence of these two components provides strong evidence for the existence of at least two recombination centres in the synthetic quartz studied here. The TR-OSL data in figure 4 contain also a much slower luminescence component with a lifetime

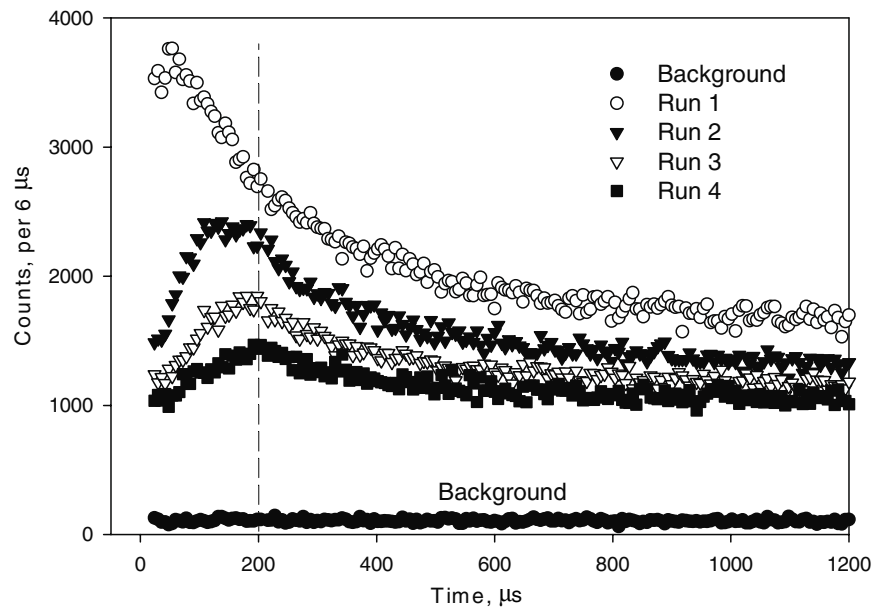


Figure 4. A different type of TR-OSL data for annealed synthetic quartz; the overall signal in each cycle increases initially and then decreases while the LED stimulation is still on. Note also that the time t_{\max} corresponding to the maximum of the luminescence signal shifts systematically from $\sim 50 \mu\text{s}$ for cycle 1 to $\sim 190 \mu\text{s}$ for cycle 4. All graphs can be fitted with two decaying exponentials. The resulting time constant τ_1 of the first fast component is constant for all cycles with an average value of $\tau_1 = (180 \pm 50) \mu\text{s}$, and is most likely identical to the fast component found in figure 3, which has a lifetime of $\tau_f = (132 \pm 4) \mu\text{s}$. The lifetime for the second slow component in the data is very long, with an average value of $\tau_2 = (14 \pm 8) \text{ms}$. This large lifetime may be due to the phenomenon of delayed OSL (DOSL).

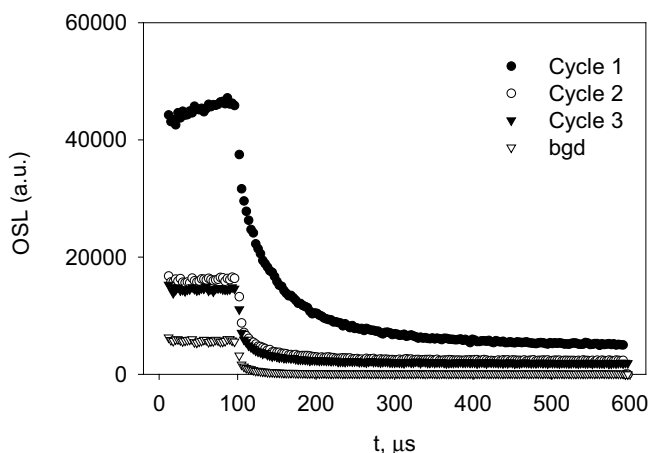


Figure 5. An example of TR-OSL data obtained from annealed and irradiated marble powder samples. The decaying part of the data (after the LED was turned off) can be fitted to a single exponential plus a constant. The luminescence lifetimes decrease steadily from cycle 1 to cycle 5, from $\tau = 62 \mu\text{s}$ for cycle 1 to $\tau = 19 \mu\text{s}$ for cycle 5.

of $\tau_2 = (14 \pm 8) \text{ms}$, which can be attributed to the DOSL phenomenon previously reported in quartz.

3.3. TR-OSL data for annealed marble

Figure 5 shows an example of TR-OSL data obtained from marble powder samples of Greek origin. The powder samples were annealed for 1 h at 900°C in order to enhance their sensitivity and irradiated with a nominal dose of 20 Gy. The OSL intensity was measured for four consecutive cycles consisting of 100 000 scans each, followed by a 15 s interval.

The decaying part of the data in figure 5 (after the LED was turned off) was fitted to a single exponential plus a constant. The lifetimes obtained from the decaying exponential fits decreased steadily from a value of $\tau = 62 \mu\text{s}$ for cycle 1 to a value of $\tau = 19 \mu\text{s}$ for cycle 5. It is noted that this data could also be fitted with the sum of two exponentials with approximately the same fitting accuracy, as judged by the value of the correlation coefficients ($R \sim 0.90$ in both cases). Galloway [25] studied TR-OSL from limestone samples and identified two luminescence components at room temperature with lifetimes of 5 and $35 \mu\text{s}$. When their limestone samples were optically stimulated at temperatures higher than 100°C , it was found that only the fast component survived.

3.4. TR-OSL data and TL glow curves for beta irradiated iodized salt

Figure 6 shows TR-OSL measurements for a commercially available iodized sea salt sample (brand name KALASTM). This sample was found to exhibit a very high OSL sensitivity to beta irradiation, similar to the high sensitivity reported previously by Bailey *et al* [18]. To the best of our knowledge, there have been no previously reported TR-OSL measurements in the literature for beta irradiated salt. The salt sample was irradiated for 1 min with a nominal dose of 2 Gy, the background signal in this example being again negligible, and the TR-OSL intensity was measured for six consecutive cycles as described previously. The data in figure 6 exhibit the same nonmonotonic behaviour of the signal as in the quartz data of figure 4, with one important difference. In the case of figure 6 the time t_{\max} at which the luminescence signal reaches a maximum *decreases* systematically from

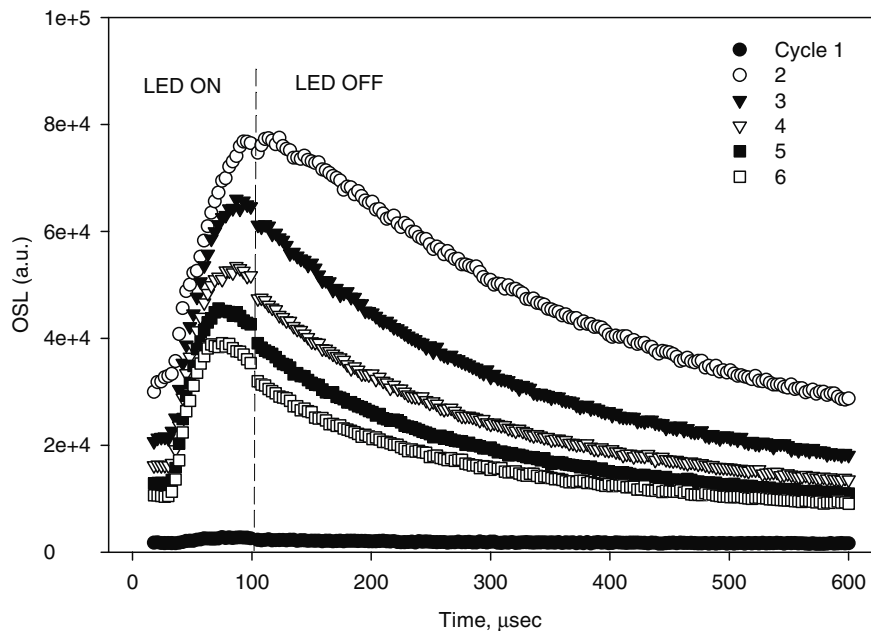


Figure 6. TR-OSL data for a commercially available iodized sea salt sample. These data also exhibit the nonmonotonic behaviour of the signal for each successive cycle while the LED is on, but in this case the time t_{\max} at which the luminescence signal reaches a maximum decreases systematically from $\sim 90 \mu\text{s}$ for cycle 1 to $\sim 70 \mu\text{s}$ for cycle 6.

$\sim 90 \mu\text{s}$ for cycle 1 to $\sim 70 \mu\text{s}$ for cycle 6. This is again a new result not previously reported for salt samples, and indicates that a different relaxation mechanism must be taking place during pulsed luminescence experiments in salt than in the quartz samples studied. A possible mechanism for this unusual behaviour most probably involves competition effects between several competing traps and luminescence centres in this material.

In a separate experiment, the relationship between the TL peaks and the measured OSL signals in beta irradiated salt was investigated as follows. Figure 7 shows twelve TL glow curves for a NaCl, common salt sample irradiated for 30 s with a nominal beta dose of 1 Gy; these twelve glow curves were measured using 12 narrow interference filters between 400 and 580 nm. The TL glow curves were measured immediately after the end of irradiation, and contain apparent TL peaks at ~ 68 , ~ 90 and $\sim 193^\circ\text{C}$ as recorded with a heating rate of $\beta = 2 \text{ K s}^{-1}$. A possible fourth TL peak appears as a small shoulder at $\sim 150^\circ\text{C}$ in some of the glow curves. Each data point shown in figure 7 is the average of 3 runs; the reproducibility of the data is very good, with the standard deviation of the data in figure 7 represented by the size of the open circles. The TL glow curves presented in figure 7 have been corrected for the quantum efficiency of the 9635QA photomultiplier tube (as provided by the manufacturer) and for the transmission efficiency of each filter.

Figure 8(a) shows the maximum TL intensity for the peaks at 68 and 193°C as a function of the transmission wavelength of the interference filters. The data in figure 8(a) show two broad luminescence bands; the first band is centred at $\sim 450 \text{ nm}$ and the second broad band extends in the region 480–580 nm. These results for the recombination centres are consistent with the values previously reported in the literature for NaCl (McKeever [26, p 173–7]) and references therein.

Numerous studies of TL glow curves in alkali halides have shown the presence of two luminescence bands at ~ 400 and $\sim 595 \text{ nm}$. These luminescence centres have been attributed to the presence of Mn^{2+} impurities in the NaCl samples.

Figure 8(b) shows the results of a bleaching experiment carried out for different bleaching times. The TL glow curves in figure 8(b) were recorded with a 580 nm interference filter, which corresponds to the broad wavelength region of the second luminescence centre (500–600 nm) present in the salt samples. After a 1 Gy irradiation, the salt sample was exposed to the full power illumination using the blue LEDs (470 nm), and for the times indicated in the legend of figure 8(b). The TL peak at $\sim 68^\circ\text{C}$ becomes completely bleached after short illumination times ($t \sim 30 \text{ s}$), while the TL peaks at ~ 90 and $\sim 193^\circ\text{C}$ show a fast initial decline, followed by a much slower bleachable component. Very similar results were obtained using a 450 nm interference filter, which corresponds to the wavelength region of the first luminescence centre.

The TL data in this section are important in understanding the origin of the TR-OSL signal in salt and how this signal is related to the TL/OSL data available on this material. Furthermore, the TL spectra in figures 7 and 8(a) provide information on the number and relative importance of the recombination centres in salt samples.

4. A kinetic model for pulsed OSL in quartz

4.1. Previous modelling work for pulsed OSL in quartz

It has been well established that the luminescence processes in quartz are very complex, with many energy levels contributing in the experimentally observed OSL signals (see, e.g. [27–29]). While these modelling efforts have provided descriptions of several TL, CW-OSL and LM-OSL measurements, there have

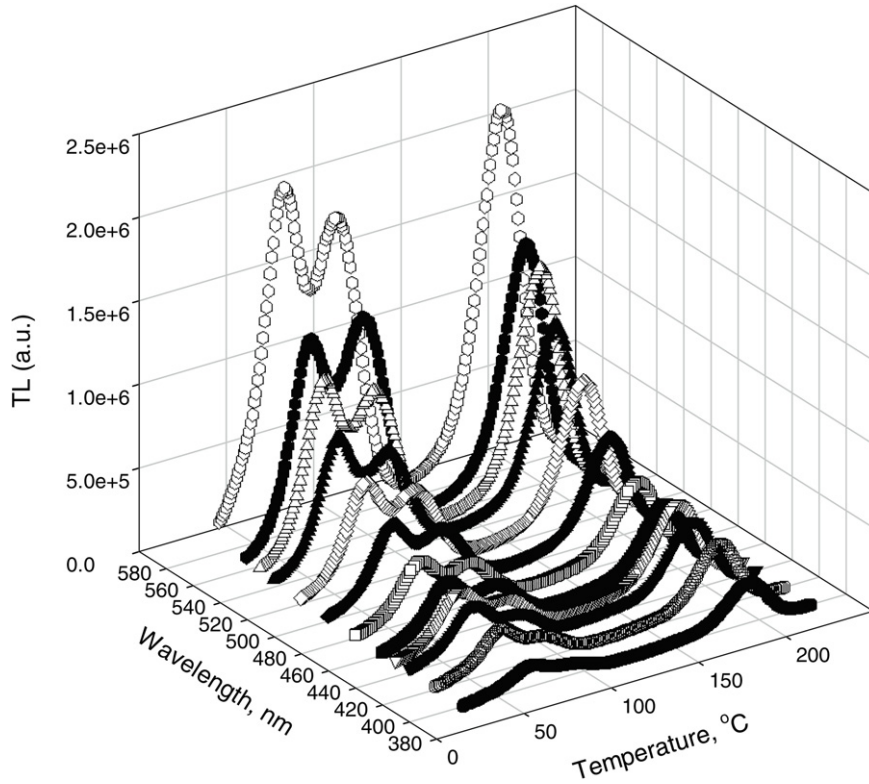


Figure 7. The TL glow curves for a salt sample irradiated with a beta dose of 1 Gy; the glow curves were measured using narrow interference filters between 400 and 600 nm, in intervals of 20 nm. The TL glow curves contain TL peaks at 75, 120 and 230 °C and each data point shown here is the average of 3 runs, with the standard deviation of the data represented by the size of the open circles. The TL glow curves have been corrected for the quantum efficiency of the photomultiplier tube and for the transmission efficiency of each filter. The sample was heated at a rate of 2 K s⁻¹.

been very few attempts at developing quantitative models for TR-OSL.

Chithambo [4, 5] developed a model for the time dependence of luminescence emission from quartz. The model shows that during stimulation of electrons from a trap with an initial electron population A and with a probability of stimulation per unit time s , the time dependence of the number of stimulated electrons $N(t)$ is given by an exponential rise of the form

$$N(t) = \frac{sA}{\lambda} (1 - e^{-\lambda t}), \quad (1)$$

where λ is the probability per unit time that a stimulated electron will produce luminescence during the excitation pulse. Within this model, after the luminescence stimulating pulse is turned off, the luminescence decays exponentially as

$$L(t) = \lambda N(t_1) e^{-(t-t_1)\tau}, \quad (2)$$

where τ is the lifetime of the decay and t_1 is the width of a short rectangular pulse.

Chithambo [6] studied TR-OSL signals from low sensitivity natural quartz from crystalline rock and found considerable variation in the values of the principal luminescence lifetimes for various types of quartz. They attributed these large variations to different thermal histories of the samples, and explained their results in terms of a model consisting of three luminescence centres, with the

thermal history of the sample possibly linked to the hole concentration of the centres. The energy band diagram of Chithambo [6] contains STs, optically sensitive traps (OSTs), deep traps (DTs) which cannot be optically stimulated and some levels representing self-trapped excitons (STEs). Within this model, the influence of thermal annealing on lifetimes can be explained by the transfer of holes during annealing from a non-luminescent centre R to the three luminescence centres available in the model. This process of hole transfer has been well documented previously in both experimental and theoretical studies of quartz [30]. A similar qualitative model was discussed recently by Ogundare and Chithambo [15], who studied the luminescence lifetimes and TR-OSL intensity of annealed and unannealed quartz samples from Nigeria. These authors interpreted their experimental results by using a model consisting of three luminescence centres. They suggested that the probability of hole trapping during irradiation may be highest for the luminescence centre associated with the least lifetime. Their model consists of three electron traps, three luminescence centres and one non-radiative centre.

4.2. A new kinetic model for pulsed OSL in quartz

In this section a simple model is presented, which can reproduce several of the commonly reported shapes of the pulsed-OSL signals in quartz. It will be shown that the model can reproduce a quantitative description of the shapes

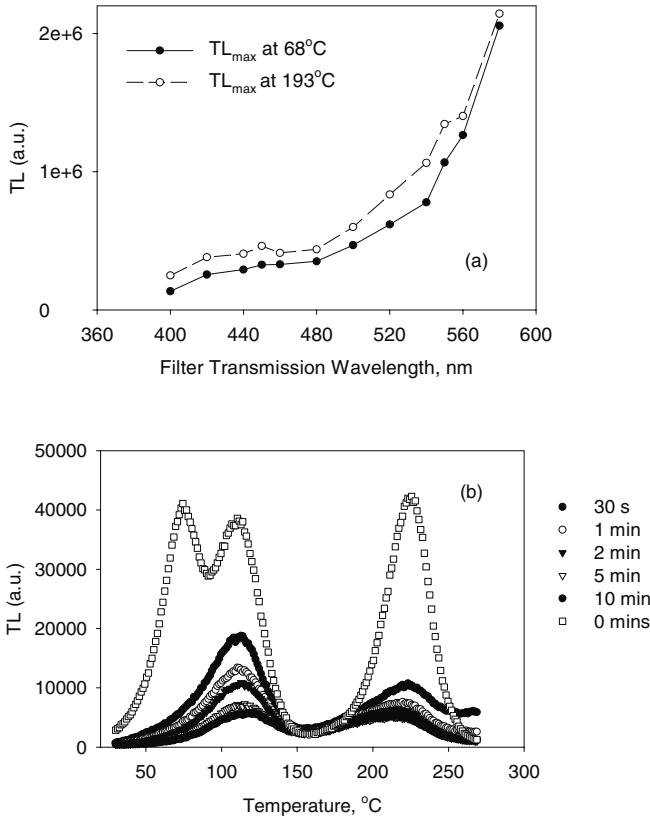


Figure 8. (a) The maximum TL intensity of the peaks at 68 and 193 °C as a function of the transmission wavelength of the interference filters. The data show two broad luminescence bands, with the first band centred at ~450 nm and the second broad band extending in the region 480–580 nm. (b) A bleaching experiment carried out for different bleaching times indicated in the legend. The TL glow curves shown were recorded with a 580 nm filter. Very similar results were obtained using a 450 nm interference filter.

of the TR-OSL data, both during stimulation and during the relaxation process. The model presented in this section is certainly a simplification of the actual physical situation; its value consists of being able to demonstrate the various experimental shapes of the TR-OSL signal, and in providing valuable insights in the complex competition processes taking place in the quartz samples.

The model is shown schematically in its most general form in figure 9, and consists of the main electron trap T and three luminescence centres L1, L2, L3. The system of differential equations to be solved during the stimulation pulse is

$$\frac{dn_1}{dt} = -\lambda n_1(t) + A_n(N_1 - n_1(t))n_c(t), \quad (3)$$

$$\frac{dm_1}{dt} = -A_{m1}m_1(t)n_c(t), \quad (4)$$

$$\frac{dm_2}{dt} = -A_{m2}m_2(t)n_c(t), \quad (5)$$

$$\frac{dm_3}{dt} = -A_{m3}m_3(t)n_c(t), \quad (6)$$

$$\frac{dn_c}{dt} = \frac{dm_1}{dt} + \frac{dm_2}{dt} + \frac{dm_3}{dt} - \frac{dn_1}{dt}. \quad (7)$$

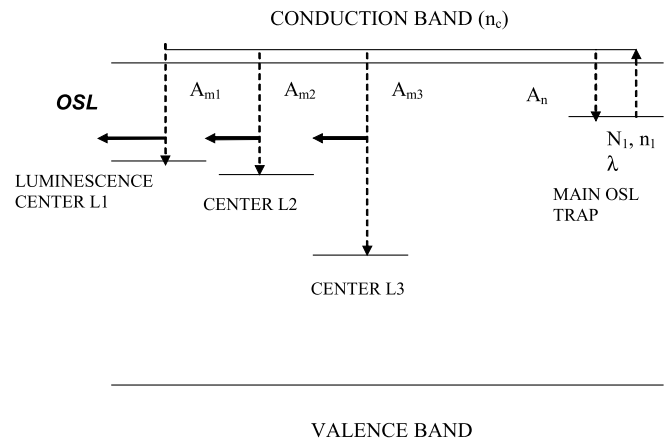


Figure 9. The energy levels in the kinetic model for quartz, consisting of a single electron trap T and three recombination centres L1, L2 and L3.

The instantaneous luminescence is defined as

$$L = -\frac{dm_1}{dt} - \frac{dm_2}{dt} - \frac{dm_3}{dt}. \quad (8)$$

After the LED pulse is turned off, the system of equations remains the same, except that the first equation is changed by setting the light stimulation $\lambda = 0$:

$$\frac{dn_1}{dt} = A_n(N_1 - n_1(t))n_c(t). \quad (9)$$

In the above equations N_1 and n_1 are the total and instantaneous concentrations of the trap T and m_1 , m_2 , m_3 are corresponding instantaneous concentrations of all three recombination centres. n_c is the concentration of electrons in the conduction band. The term ‘instantaneous concentrations’ refers to the number of traps actually populated by electrons or holes at any time t . The pulsed-OSL constant λ is given by $\lambda = \sigma I_0$ (s⁻¹) where σ is the photoionization cross section and I_0 represents the intensity of the stimulating light. The first term $-\lambda n_1(t)$ in equation (3) expresses the optical excitation of the electrons out of the trap, while the second term $A_n(N_1 - n_1(t))n_c(t)$ expresses the possibility of retrapping of electrons into the trap with probability A_n . Here A_{m1} , A_{m2} and A_{m3} are the probabilities of capturing electrons from the conduction band into the recombination centres. Equation (7) expresses the conservation of charge in the system and equation (8) is based on the assumption that all three recombination centres contribute to the observed pulsed-OSL signal. This assumption is consistent with the qualitative models suggested by Chithambo *et al* [14] and Ogundare and Chithambo [15].

4.3. Results of the simulations and quantitative fits to the data

4.3.1. Quantitative fit of the data of figure 2. Figure 10(a) shows the results of running the simulation with the following set of parameters: $N_1 = 10^9$ cm⁻³, $n_{10} = 10^9$ cm⁻³, $A_n = 8 \times 10^{-6}$ cm³ s⁻¹, $m_{10} = 9 \times 10^7$ cm⁻³, $m_{20} = 0$, $m_{30} = 0$, $A_{m1} = 1.75 \times 10^{-4}$ cm³ s⁻¹, $A_{m2} = 0$, $A_{m3} = 0$ and $\lambda = 10^3$ s⁻¹. It is noted that the centres L2 and L3 play no role

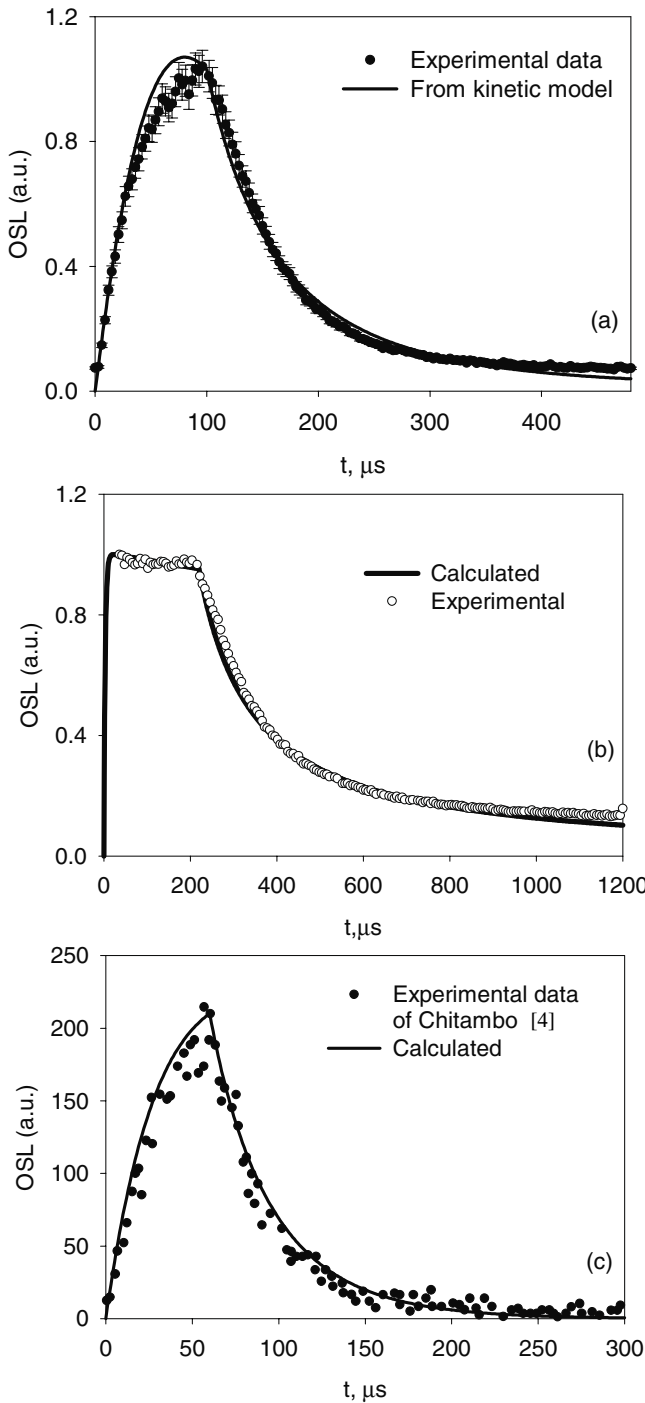


Figure 10. (a) Comparison of the simulation results from the kinetic model for quartz with the experimental data previously shown in figure 2. (b) Comparison of the simulation results for a slightly different set of parameters with the experimental data for quartz previously shown in figure 3. (c) Comparison of the simulation results for a third set of parameters with the experimental data previously published by Chithambo in figure 2 of [5]. All parameters used in the model are given in the text.

in this simulation, since $A_{m2} = A_{m3} = 0$. Here n_{10} and m_{10} are the initial concentrations of electrons and holes in the main trap and luminescence centre correspondingly. Conservation of charge requires that the concentrations of free electrons and free holes in the system balance each other out. The above

values of n_{10} and m_{10} do not balance each other out, but this does not represent an unrealistic physical situation. As is common in this type of kinetic model, it may be assumed that additional charges exist in other traps and/or recombination centres in the quartz sample, leading to a balance of charge. The results of this simulation are compared directly with the experimental data for quartz previously shown in figure 2. Both the experimental data and the simulation results were normalized to a maximum height of 1 for comparison purposes.

The error bars shown in figure 10(a) were obtained from a statistical analysis of the experimental data and of the background signal, assuming that the standard deviation of individual data points is represented by the square root of the number of counts. The statistical accuracy of the data in figure 8(a) is in the range 1–4%.

4.3.2. Quantitative fit of the data of figure 3. Figure 10(b) shows the results of running the simulation with a slightly different set of parameters: $N_1 = 10^9 \text{ cm}^{-3}$, $n_{10} = 10^9 \text{ cm}^{-3}$, $A_n = 8 \times 10^{-6} \text{ cm}^3 \text{ s}^{-1}$, $m_{10} = m_{30} = 0$, $m_{20} = 1 \times 10^7 \text{ cm}^{-3}$, $A_{m1} = A_{m3} = 0$, $A_{m2} = 25 \times 10^{-7} \text{ cm}^{-3}$ and $\lambda = 300\,000 \text{ s}^{-1}$. The results of this simulation are compared directly with the experimental data for quartz previously shown in figure 3.

4.3.3. Quantitative fit of the data of Chithambo [5]. Figure 10(c) shows the results of running the simulation with a third different set of parameters: $N_1 = 10^9 \text{ cm}^{-3}$, $n_{10} = 10^9 \text{ cm}^{-3}$, $A_n = 8 \times 10^{-6} \text{ cm}^3 \text{ s}^{-1}$, $m_{10} = 5 \times 10^9 \text{ cm}^{-3}$, $m_{20} = 0$, $m_{30} = 0$, $A_{m1} = 6.1 \times 10^{-4} \text{ cm}^{-3}$, $A_{m2} = 0$, $A_{m3} = 0$ and $\lambda = 200 \text{ s}^{-1}$. The results of this simulation are compared directly with the experimental data previously published by Chithambo in figure 2 of [5]. It is noted that Ogundare and Chithambo [15] fitted an exponential decay function to the experimental data of figure 10(c) and obtained the value of the lifetime $\tau = (31.6 \pm 0.8) \mu\text{s}$.

The three examples shown in figure 10 demonstrate that the kinetic model presented in this section can successfully simulate the three different experimental behaviours of quartz samples. The main advantages of the present kinetic model over the alternative model used by Chithambo [4] are (a) the model simultaneously describes both regions of the TR-OSL data when the stimulation is on and off and (b) further insight is obtained into the complex kinetic TR-OSL mechanisms involved in quartz.

4.4. Modelling demonstration of the nonmonotonic behaviour of the TR-OSL signal

Figure 11 shows a modelling demonstration of the nonmonotonic behaviour of the pulsed-OSL signal shown in figure 5 for synthetic quartz. The set of parameters used for this simulation is $N_1 = 10^{10} \text{ cm}^{-3}$, $n_{10} = 10^9 \text{ cm}^{-3}$, $A_n = 0$, $m_{10} = m_{30} = 0$, $m_{20} = 3.5 \times 10^5 \text{ cm}^{-3}$, $A_{m1} = 0$, $A_{m2} = 25 \times 10^{-7} \text{ cm}^{-3}$, $A_{m3} = 0$ and $\lambda = 150\,000 \text{ s}^{-1}$. The same kinetic model is run for seven different values of the initial concentration of electrons and holes in the main trap and in the luminescence centre (n_{10} and m_{10} correspondingly). The modelling results in figure 11 clearly show the shift of the value

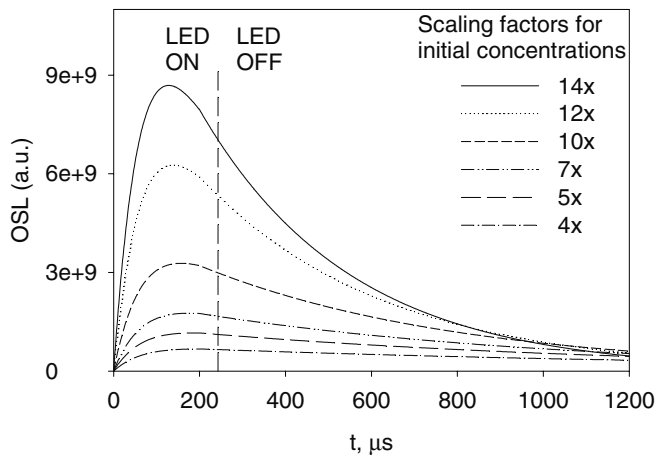


Figure 11. Modelling demonstration of the nonmonotonic behaviour of the pulsed-OSL signal shown in figure 5 for synthetic quartz. The kinetic model is run for seven different values of the initial concentration of electrons and holes in the main trap and in the luminescence centre (n_{10} and m_{10} correspondingly). The modelling results clearly show the shift of the value of t_{\max} from $\sim 120 \mu\text{s}$ to $\sim 190 \mu\text{s}$ as the initial concentrations n_{10} and m_{10} are reduced by the scaling factors indicated in the legend.

of t_{\max} from ~ 120 to $\sim 190 \mu\text{s}$ as the initial concentrations n_{10} and m_{10} are reduced by the scaling factors indicated in the legend of figure 11.

We have not attempted a quantitative fit of the experimental data for marble and salt shown in figures 5 and 6, since not enough information is available concerning the number and types of recombination centres in these materials.

The different shapes of the simulated data in figures 10(a), (b) and 11 are due to the presence of several recombination centres, as shown in the model of figure 9. These centres have different recombination probabilities and hole populations, which affect the shape of the TR-OSL data. Extensive experimental TR-OSL work on quartz has shown that the relative influence of such recombination centres depends on the thermal history and on the irradiation history of the quartz samples (see, e.g., [6, 11, 15, 25]). In several of these previous studies a change in measured lifetimes with annealing temperature was interpreted on the basis of changing hole concentrations due to the annealing process. Such a change in measured lifetimes results in a change in shape of a TR-OSL spectrum. In general, however, the shape of the TR-OSL spectrum of quartz and the corresponding luminescence lifetime can be influenced by a complex array of factors including the type and number of centres, the thermal history and provenance of the samples [14], and possible changes in the concentration of recombination centres [6]. The experimental data in figure 3 and the corresponding simulation in figure 10(b) suggest that the intensity of the stimulating light may also be a contributing factor determining the shape of TR-OSL data for annealed quartz, with very high stimulating light intensities resulting in a faster approach to saturation, as shown in figure 3.

At first sight, it is rather surprising that different aliquots of the same sample should produce the different curves shown in figures 2–4. Our modelling results show that the different

shapes are due to the prevalence of different recombination centres for different aliquots. This in turn is due to the strong dependence of the TR-OSL shape on the following factors: thermal and irradiation history of the sample, the dose given to the samples prior to TR-OSL measurement, the hole concentrations in the centres and on the stimulating light intensity used during the experiment. For example, the rising part of the experimental data in figure 2 is dominated by a luminescence component with a medium lifetime of $\sim 34 \mu\text{s}$. On the other hand, the experimental data in figure 3 are dominated by much faster components that reach saturation within the first $25 \mu\text{s}$ of the TR-OSL signal. Even though the component with a medium lifetime of $\sim 34 \mu\text{s}$ seems to be absent in figure 3, it is actually present, but is of much smaller intensity than the faster components. Finally the experimental data in figure 4 seem to show an intermediate situation between figures 2 and 3, and perhaps a gradual transition between the two situations in figures 2 and 3. We estimate that the different TR-OSL shapes shown in figures 2–4 will be most easily observable for freshly annealed samples which were given rather low doses (1–2 Gy).

The ultimate physical reason for the nonmonotonic effect shown in figure 4 are the competition effects occurring between the luminescence centres shown in figure 9. Rather extensive experimental work has shown that high temperature annealing of quartz samples above $\sim 500^\circ\text{C}$ activates different luminescence centres, with the actual luminescence lifetime depending on the annealing temperature (see, e.g., [6] and references therein). Furthermore, irradiating or additional annealing of the same quartz samples has been shown to result in additional changes in the measured luminescence lifetimes [6, 11]. Depending on the pre-measurement annealing, even small changes in dose produce noticeable changes in the shape of spectra and in the corresponding luminescence lifetimes (e.g. [6]).

It should also be noted that during the stimulating light pulse the time dependence of the luminescence is influenced by both the shape of the light pulse and the luminescence lifetime, whereas after the end of the light pulse only the luminescence lifetime is relevant [11]. For example, if for some reason, the luminescence during stimulation is a negligible proportion of the signal then the signal will tend to be dominated by the constant intensity pulse and assume its shape. This feature was demonstrated for successive pulsed measurements made on an aliquot of quartz ([11], figure 9(a)). A similar characteristic is sometimes observed if the pulse width is much longer than the characteristic lifetime of the sample (as was shown for microcline feldspar in [11], figure 6).

It must be emphasized that the nonmonotonic effect described in this paper is very different in nature from the nonmonotonic *dose dependence* of OSL which has been previously discussed by Pagonis *et al* [31].

5. Conclusions

This paper presented several types of TR-OSL data for annealed high purity synthetic quartz; the experimental data are consistent with the presence of at least two exponential

components with average lifetimes of $\tau_d = (61.1 \pm 0.6) \mu\text{s}$ and $\tau_f = (132 \pm 4) \mu\text{s}$. The presence of these two components provides strong evidence for the existence of at least two recombination centres in the synthetic quartz studied here, in general agreement with several other published studies of quartz samples. The TR-OSL data in figure 4 also contain a much slower luminescence component with a lifetime of $\tau_2 = (14 \pm 8) \text{ms}$, which can be attributed to the DOSL phenomenon previously reported in quartz and other dosimetric materials.

Additional TR-OSL data were presented for annealed marble, and for commercially available iodized salt. A new type of nonmonotonic behaviour for TR-OSL signals for quartz and iodized salt is presented which occurs during optical stimulation; this type of behaviour was explained for quartz samples using a rather simple model consisting of one main OSL trap and several recombination centres. The same model was used to quantitatively fit several sets of experimental data for quartz.

Acknowledgments

The financial support provided by Dr Thomas Falkner, Provost and Dean of Faculty at McDaniel College, by the Kopp research fund at McDaniel College, by the Sue Sunger Research Fund at McDaniel College and by the Faculty Development Committee at McDaniel College are gratefully acknowledged. We also thank two anonymous referees for their comments which contributed to the improvement of the manuscript.

References

- [1] Wintle A G and Murray A S 2006 *Radiat. Meas.* **41** 369–91
- [2] Bulur E, Bøtter-Jensen L and Murray A S 2001 *Radiat. Meas.* **33** 715–9
- [3] Bøtter-Jensen L, McKeever S W S and Wintle A G 2003 *Optically Stimulated Luminescence Dosimetry* (Amsterdam: Elsevier)
- [4] Chithambo M L 2007a *J. Phys. D: Appl. Phys.* **40** 1874–9
- [5] Chithambo M L 2007b *J. Phys. D: Appl. Phys.* **40** 1880–9
- [6] Chithambo M L 2003 *Radiat. Meas.* **37** 167–75
- [7] Chithambo M L 2006 *Radiat. Meas.* **41** 862–5
- [8] Sanderson D C W and Clark R J 1994 *Radiat. Meas.* **23** 633–9
- [9] Clark R J and Bailiff I K 1998 *Radiat. Meas.* **29** 553–60
- [10] Clark R J, Bailiff I K and Tooley M J 1997 *Radiat. Meas.* **27** 211–20
- [11] Chithambo M L and Galloway R B 2000 *Meas. Sci. Technol.* **11** 418–24
- [12] Tsukamoto S, Denby P M, Murray A S and Bøtter-Jensen L 2006 *Radiat. Meas.* **41** 790–5
- [13] Denby P M, Bøtter-Jensen L, Murray A S, Thomsen K J and Moska P 2006 *Radiat. Meas.* **41** 774–9
- [14] Chithambo M L, Preusser F, Ramseyer K and Ogundare F O 2007c *Radiat. Meas.* **42** 205–12
- [15] Ogundare F O and Chithambo M L 2007 *Opt. Mater.* **29** 1844–51
- [16] Murthy K V R, Pallavi S P, Rahul G, Patel Y S, Sai Prasad A S and Elangovan D 2006 *Radiat. Prot. Dosim.* **119** 350–2
- [17] Ankjærgaard C, Murray A S, Denby P M and Bøtter-Jensen L 2006 *Radiat. Meas.* **41** 780–6
- [18] Bailey R M, Adamiec G and Rhodes E J 2000 *Radiat. Meas.* **32** 717–23
- [19] Thomsen K J, Bøtter-Jensen L and Murray A S 2002 *Radiat. Prot. Dosim.* **101** 515–8
- [20] Markey B G, Colyott L E and McKeever S W S 1995 *Radiat. Meas.* **24** 457–63
- [21] Akselrod M S and McKeever S W S 1999 *Radiat. Prot. Dosim.* **81** 167–76
- [22] Charitides C, Kitis G, Furetta C and Charalambous S 2000 *Nucl. Instrum. Methods Phys. Res. B* **168** 404–10
- [23] Kitis G, Pagonis V, Chen R and Polymeris G 2006 *Radiat. Prot. Dosim.* **119** 438–41
- [24] Polymeris G, Kitis G and Pagonis V 2006 *Radiat. Meas.* **41** 554–64
- [25] Galloway R B 2003 *Radiat. Meas.* **37** 177–85
- [26] McKeever S W S 1985 *Thermoluminescence in Solids* (Cambridge: Cambridge University Press)
- [27] Bailey R M 2001 *Radiat. Meas.* **33** 17–45
- [28] Bailey R M 2004 *Radiat. Meas.* **38** 299–310
- [29] Adamiec G, Bluszcz A, Bailey R and Garcia-Talavera M 2006 *Radiat. Meas.* **41** 897–902
- [30] Chen R and McKeever S W S 1997 *Theory of Thermoluminescence and Related Materials* (Singapore: World Scientific)
- [31] Pagonis V, Chen R and Lawless J 2006 *Radiat. Meas.* **41** 903–9